Obrabotka metallov (tekhnologiya, oborudovanie, instrumenty) = Metal Working and Material Science. 2023 vol. 25 no. 2 pp. 68–80
ISSN: 1994-6309 (print) / 2541-819X (online)
DOI: 10.17212/1994-6309-2023-25.2-68-80

NSTU NETI

Obrabotka metallov - Metal Working and Material Science

Journal homepage: http://journals.nstu.ru/obrabotka_metallov

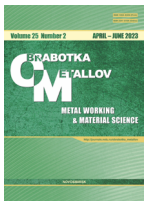

In-situ analysis of ZrN/CrN multilayer coatings under heating

Andrey Vorontsov [1, a], Andrey Filippov [1, b,], Nikolay Shamarin [1, c], Evgenij Moskvichev [1, d], Ol'ga Novitskaya [1, e], Evgenii Knyazhev [1, f], Yuliya Denisova [2, g], Andrei Leonov [2, h], Vladimir Denisov [2, i]*

[1] Institute of Strenght Physics and Materials Sciences SB RAS, 2/4 pr. Academicheskii, Tomsk, 634055, Russian Federation
[2] Institute of High Current Electronics SB RAS, 2/3 per. Academicheskii, Tomsk, 634055, Russian Federation

[a] https://orcid.org/0000-0002-4334-7616, vav@ispms.ru, [b] https://orcid.org/0000-0003-0487-8382, andrey.v.filippov@yandex.ru,
[c] https://orcid.org/0000-0002-4649-6465, shnn@ispms.ru, [d] https://orcid.org/0000-0002-9139-0846, em_tsu@mail.ru,
[e] https://orcid.org/0000-0003-1043-4489, nos@ispms.tsc.ru, [f] https://orcid.org/0000-0002-1984-9720, zhenya4825@gmail.com,
[g] https://orcid.org/0000-0002-3069-1434, yukolubaeva@mail.ru, [h] https://orcid.org/0000-0001-6645-3879, laa-91@yandex.ru,
[i] https://orcid.org/0000-0002-5446-2337, volodyadenisov@yandex.ru

ARTICLE INFO

Article history:
Received: 15 March 2023
Revised: 22 March 2023
Accepted: 28 March 2023
Available online: 15 June 2023

Keywords:
Coating
Nitrides
Phase composition
RSA
CTE
Stresses

Funding
The work was carried out with the financial support of the Russian Federation represented by the Ministry of Science and Higher Education (project No. 075-15-2021-1348) within the framework of event No. 1.1.16.

Acknowledgements
Research were partially conducted at core facility "Structure, mechanical and physical properties of materials"

ABSTRACT

Introduction. Advanced hard coatings combine different properties such as high hardness, wear resistance, corrosive resistance. At present, layer-by-layer deposited zirconium and chromium nitrides are promising hard coating materials. Currently, the multilayer coating process is not sufficiently described in the literature to understand all the processes involved. The problem is the complexity of depositing thick layers of multilayer, multicomponent coatings with different physical characteristics of the coating components. First and foremost this concerns the *coefficient of linear thermal expansion* (*CTE*). Since the coating and operating processes consist in heating, coating components with different *CTE* will be susceptible to cracking, further failure and product failure over time. **The purpose** of work is in-situ study of multilayer *ZrN*/*CrN* coatings by X-ray analysis using synchrotron radiation and qualitative microstress behavior of multilayer coatings formed by plasma-assisted vacuum-arc method on substrate of alloy *VK8* (92% *WC*–8% *Co*) under heating up to 750°C. **Research methodology.** Samples of coatings made of chromium and zirconium nitrides deposited on a substrate of the hard alloy *VK8* are investigated. The basic method is the X-ray analysis using synchrotron radiation. We used the most common techniques to study the characteristics of multilayered coatings such as the *coefficient of linear thermal expansion* and *the qualitative measurement of microstresses*. **Results and discussion.** The result is the ability to determine changes in the characteristics of multilayer coatings during heating, such as changes in the crystal lattice parameter of each of the coating components separately, the possibility to determine the *coefficient of linear thermal expansion* of the coating components and the *qualitative measurement of microstresses*, as well as providing the opportunity, based on the analysis, to form recommendations for further application of the technology of applying multilayer coatings with given characteristics.

For citation: Vorontsov A.V., Filippov A.V., Shamarin N.N., Moskvichev E.N., Novitskaya O.S., Knyazhev E.O., Denisova Yu.A., Leonov A.A., Denisov V.V. In-situ analysis of ZrN/CrN multilayer coatings under heating. *Obrabotka metallov (tekhnologiya, oborudovanie, instrumenty) = Metal Working and Material Science*, 2023, vol. 25, no. 2, pp. 68–80. DOI: 10.17212/1994-6309-2023-25.2-68-80. (In Russian).

*** Corresponding author**
Vorontsov Andrey V., Ph.D. (Engineering), Junior researcher
Institute of Strenght Physics and Materials Sciences SB RAS,
2/4 pr. Academicheskii,
634055, Tomsk, Russian Federation
Tel.: 8 (983) 239-34-17, **e-mail:** vav@ispms.ru

Introduction

With the development of materials production technology for cutting tools, press molds, engine components, and other mechanical components, mainly hard coatings are used [1, 2]. Metal nitrides such as chromium, niobium, zirconium, tantalum, titanium, or its combinations are primarily used as coating materials [3–5]. Such coatings are able to withstand the high load and temperature that characterize the operation of the cutting tool. It is worth noting that coatings are used not only to provide the necessary characteristics of cutting tools; as studies show, some coatings such as *CrN* can be used as a coating for zirconium alloy for use in fuel accident-resistant materials [6, 7], and *ZrC*/*TaC*, *Ru-Al*/*Ru-Si-Zr* finds applications in the aviation industry and gas turbine blades [8, 9].

In this regard, the main methods of coating deposition can be named as reactive magnetron sputtering [3, 10], vacuum brazing [11], thermal spraying [12], high-speed physical vapor deposition [13, 14], and pulsed electro deposition [15]. In this work, the vacuum arc plasma deposition method is used [16].

Despite the wide use of nitride coatings in the cutting tools manufacture, the limits of its application, and properties acquired after exposure to certain conditions are being investigated. In most cases, corrosion resistance [17] and oxidation processes [10, 18] at temperatures above 1,000 °C are studied. The authors [17] found that multilayer *Cr*/*CrN* coatings on a *Zr*-4 zirconium alloy substrate exhibit good resistance to steam oxidation with a decrease in the thickness of the multilayer coating layers. In turn, the primary task of characterizing the coating process is not described in the literature. The problem lies in the complexity of depositing thick multilayer, multicomponent coatings with different physical characteristics. First of all, this concerns the coefficient of linear thermal expansion (*CLTE*) of the components of the multilayer coating. Since the process of deposition and operation of coatings involves temperature exposure, the components of the coating with different *CLTEs* will eventually be prone to cracking, further destruction, and failure of the products.

The aforementioned works suggest that it is important not only to understand the characteristics and properties of nitride coatings, but also the kinetics of the structural behavior of multilayer coatings obtained through thermal action in air. Therefore, the purpose of this work is to in-situ study the patterns of structural changes in *CrN*/*ZrN* multilayer coatings deposited on a *92 wt.% Co-8 wt.% WC* substrate by vacuum-arc plasma deposition after thermal testing in air with an exposure temperature of 30 to 750 °C. The conducted research will be useful for developing knowledge on the behavior of materials with various physical properties in multilayer coatings at elevated operating temperatures in engineering applications, such as cutting tools. The study is based on the task of investigating the structural-phase composition in *CrN*/*ZrN* multilayer coatings during the heating of the substrate of *92 wt.% Co-8 wt.% WC* alloy with a multilayer coating consisting of alternating nitride layers of *CrN* and *ZrN*.

The aim of this study is to conduct in-situ investigation of *ZrN*/*CrN* multilayer coatings using X-ray structural analysis with synchrotron radiation and to qualitatively assess the behavior of microstrains in multilayer coatings obtained by plasma-assisted vacuum arc method on a substrate made of *92 wt.% Co-8 wt.% WC* alloy under temperature exposure up to 750 °C. The result is to provide the opportunity to determine changes in the characteristics of multilayer coatings during heating, such as the change in the lattice parameter of each component of the coating separately, the possibility of determining the coefficient of thermal expansion of the coating components, and the qualitative determination of microstrains, as well as the possibility of forming recommendations for further application of multilayer coating deposition technology with specified characteristics based on the conducted analysis.

Methods and materials

Experimental specimens subjected to heating during synchrotron investigations were used with *ZrN*/*CrN* multilayer coatings applied to a substrate of *92 wt.% Co-8 wt.% WC* alloy using a plasma-assisted vacuum arc method, obtained at different rotation speeds of the table and substrate holder in the planetary coating deposition scheme shown in Fig. 1. For the experiment, two coating deposition modes were selected: table rotation speed of 0.5 rpm (*ZrN*/*CrN-0.5* specimen) and 8.0 rpm (*ZrN/CrN-8* specimen).

In chamber 1, substrates made of *92 wt.% Co-8 wt.% WC* alloy for the deposition of multilayer coatings are attached to a rotating holder 2, installed on a rotating table 3. A turbo-molecular pump 4 creates a vacuum in chamber 1, and after reaching a vacuum of 10^{-4} Pa, inert filling gas puffing occurs through a plasma source 5 to create the required working pressure in the chamber.

When the gas discharge is ignited with a current of 40 A and a bias voltage of 700 V is applied to the substrate holder with the specimens, the substrates are heated to 400 °C. After cleaning the surface of the objects under investigation by ion bombardment and its chemical activation, a mixture of nitrogen and argon gases (90/10) puffing occurs to the desired pressure, and the arc evaporator discharges are ignited with a current of 80 A for each of it. One cathode made of the deposited material (positions 6 and 7) was installed in each evaporator, in our case these were *Cr* (99.9%) and *Zr* (99.5%).

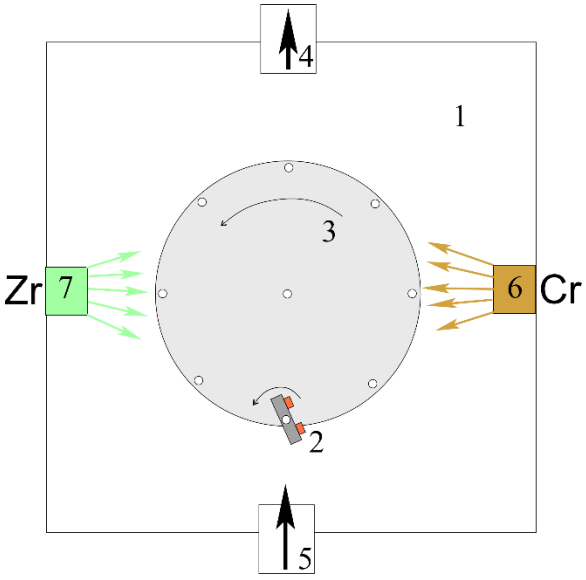

Fig. 1. Multilayer nanostructured *ZrN*/*CrN* coating application unit scheme

Specimens with multilayer coatings were circular in shape, 15 mm in diameter, and 3 mm thick, with a thickness of coatings. The thickness of the coatings was in all cases 5 μm.

The most appropriate method for the research task is in-situ synchrotron characterization of multilayer coatings during temperature exposure to a multilayer coating deposited on a substrate. Coatings applied to the *92 wt.% Co-8 wt.% WC* alloy substrate were investigated using X-ray diffraction analysis (*XRD*) with synchrotron radiation (work was carried out at *VEPP-3* synchrotron). The wavelength during synchrotron experiments was 1.54 Å. For in-situ studies, the sample with a multilayer coating was placed on a heated holder in an air atmosphere. Then the initial *XRD* pattern was obtained using an asymmetric measurement method, i.e., with a fixed angle of incidence of radiation in the range of angles 2Θ, selected depending on the material of the multilayer coating (31–48).

In the next stage, the sample was heated at a given rate, providing exposure time sufficient for step-by-step construction of the *XRD* pattern of the sample with the multilayer coating using synchrotron radiation. The temperature range of heating was determined by the real operating conditions of the coatings. Simultaneous registration and recording of *XRD* patterns with a step ensuring sufficient accuracy of identification the phase transitions and structural changes occurring during heating of the coating in the temperature range from 50 to 750 °C was made. To ensure the necessary measurement accuracy, a part of the 2Θ angle range was registered, in which one reflection of each phase of the multilayer coating was presented. The sample with the multilayer coating was heated in the temperature range from 30 °C to 750 °C with a temperature increase rate not exceeding 5 °C/min, providing exposure time sufficient for the construction of the *XRD* pattern of the sample, and with a step of 10 °C, *XRD* patterns were registered and recorded using synchrotron radiation in the X-ray range of radiation with a scanning step of 0.05 degrees and a range of angular position scanning of 2Θ from 31 to 48 degrees.

After obtaining the necessary number of X-ray diffraction patterns at different temperatures, the obtained profiles were approximated with the determination of such characteristics of the reflections of the present phases as *interplanar spacings* (*d*), *the full width at half maximum intensity* (*FWHM*) and identification of all phases in the multilayer coating within the diffraction patterns selected from the entire array of obtained patterns after visual assessment of the temperature at the phase transformations beginning. To obtain the characteristics of the reflections presented in the coating phases, the obtained X-ray diffraction profiles were approximated by the *Pseudo-Voigt* function [19].

After determining all the necessary parameters of the diffraction pattern profile, the lattice parameter (*a*) was calculated for the cubic symmetry of the *CrN* and *ZrN* phases presented in the multilayer coating, as

well as the coefficient of thermal expansion (*CLTE*) for each phase at all stages of the heating temperature range. Based on the obtained data, a dependence of the lattice parameter (*a*) for each phase of the multilayer coating on the temperature of exposure was constructed for each stage of the heating temperature range of the sample with a multilayer coating, as well as the dependence of the change in the lattice parameter (*Δa*) and graphical determination of the *CLTE* using the last coefficient of thermal expansion.

Quantitative determination of the crystal lattice parameter (*a*) was carried out after approximation and determination of interplanar distances (*d*) using equation 1 [20]:

$$a = d \cdot \sqrt{H^2 + K^2 + L^2}\,, \tag{1}$$

where *d* is the interplanar distance [Å]; *H*, *K*, *L* are the *Miller* indices of the analyzed reflection.

Based on the calculated crystal lattice parameters of the multilayer coating components using equation 1, it is possible to calculate the linear coefficient of thermal expansion (*CLTE*) of each component of the multilayer coating separately using equation 2:

$$\beta = \frac{\Delta a}{a \Delta T}, \tag{2}$$

where β is the CLTE (K^{-1}); *a* is the crystal lattice parameter in nm; Δ*a* is the change in the crystal lattice parameter in nm when the sample with the multilayer coating is subjected to a temperature change (Δ*T* [K]).

To assess the temperature at which microstresses may occur, the full width at half maximum intensity (*FWHM*) of the coating phases was plotted against temperature. As it is known from literature [21] that the magnitude of microstresses is directly proportional to *FWHM*, comparing the *FWHM* of at least two samples with multilayer coatings allows for conclusions to be drawn about the degree of microstresses present in multilayer coatings.

Results and discussion

The heating was carried out in an air medium on a holder with a platinum heating element. The initial state of the multilayer coating material was characterized by obtaining an X-ray diffraction pattern at a temperature of 30 °C. In our case, for the *CrN* and *ZrN* coating phases, the X-ray diffraction pattern registration range was 31–48 2Θ.

Figure 2 shows an array of X-ray diffraction patterns obtained at a heating rate of 5°C/min, by the asymmetric scanning method using synchrotron radiation transformed into monochromatic radiation with a wavelength of 1.54 Å, during the heating *ZrN*/*CrN*-coated samples in the temperature range from 30 °C to 750 °C. The array consists of 71 projections of X-ray diffraction patterns obtained from both the substrate surface and the layers of the deposited multilayer coating, where each projection of the diffraction pattern represents a gradation of pseudo-color, shown in Fig. 2, indicating the intensity of the obtained signal during the X-ray diffraction pattern construction. Such data visualization is convenient for a qualitative analysis of phase transformations.

The graphs presented in Fig. 2 (*a*, *b*) allow assessing the final stage of phase transitions in multilayer coatings. In the case of the *CrN*/*ZrN* coating applied at a table rotation speed of 0.5 rpm, the coating phase completely disappears at 575 °C, while the *CrN*/*ZrN* multilayer coating applied at a table rotation speed of 8 rpm completely loses its phase only at 635 °C.

Fig. 3 shows selected X-ray diffraction patterns from the array shown in Fig 2. The temperature interval, initial and final points of temperature exposure are chosen for the sake of readability of a smaller data array and considerations of the end of phase transformations. As shown in Fig. 2, coating phases in multilayer coatings completely disappear after 650 °C, and it is advisable to limit the temperature range from 30 °C to 650 °C.

In Table 1, the calculated values of interplanar spacing (*d*, Å), the width of the reflection at *FWHM* (in degrees), as well as the lattice parameter of the crystalline structure for the components of the *CrN*/*ZrN*

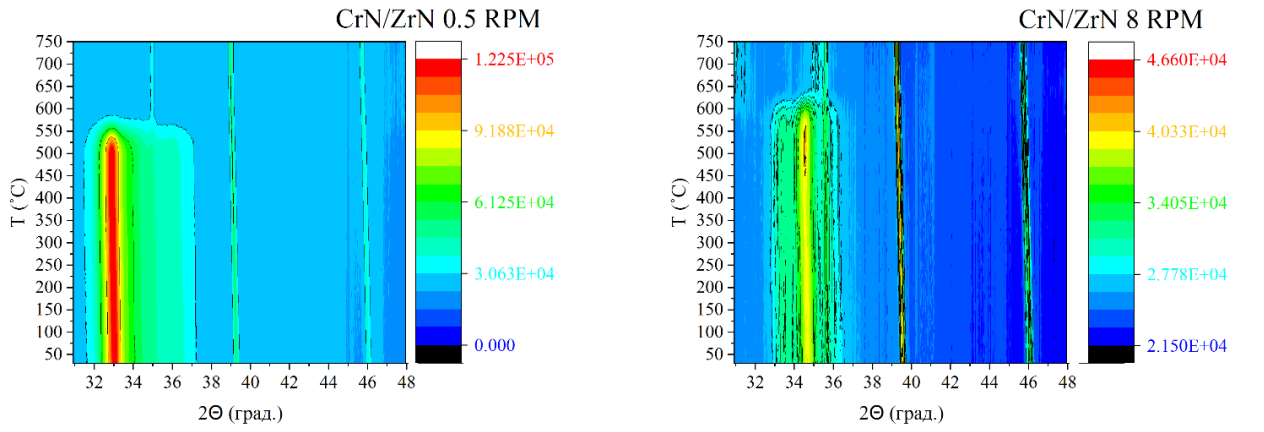

a *b*

Fig. 2. Projections of X-ray diffraction patterns, in pseudocolor gradation, denoting the signal intensity when taking X-ray diffraction patterns:
a – ZrN/CrN 0.5 rpm; *b – ZrN/CrN* 8 rpm

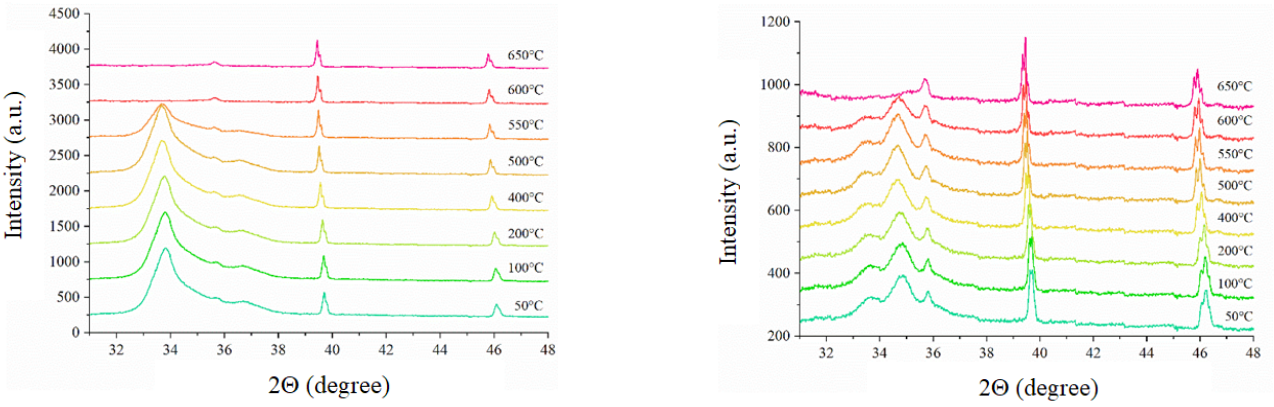

a *b*

Fig. 3. A series of X-ray diffraction patterns of an experimental sample with a multilayer ZrN/CrN coating, obtained by asymmetric imaging using synchrotron radiation when heating from 30°C to 750°C:
a – ZrN/CrN 0.5 rpm; *b – ZrN/CrN* 8 rpm

Table 1

Characteristics of phase reflections in the sample with multilayer coating of *CrN/ZrN* obtained at a substrate holder rotation speed of 0.5 rpm depending on the temperature of exposure

Temperature, °C	Reflection, phase	*d*, Å	*FWHM*, deg.	*a*, nm
50	(111) *ZrN*	2.654	1.0131	4.5965
	(111) *CrN*	2.45	1.5584	4.2426
100	(111) *ZrN*	2.653	1.0433	4.5956
	(111) *CrN*	2.44	1.3269	4.2265
200	(111) *ZrN*	2.658	0.9849	4.6030
	(111) *CrN*	2.45	1.4758	4.2428
400	(111) *ZrN*	2.662	0.9586	4.6105
	(111) *CrN*	2.456	1.5005	4.2540
500	(111) *ZrN*	2.664	0.915	4.6145
	(111) *CrN*	2.454	1.4635	4.2511
550	(111) *ZrN*	2.662	0.8375	4.6103
	(111) *CrN*	2.455	1.5585	4.2516

multilayer coating, obtained at a substrate holder rotation speed of 0.5 rpm, are presented according to the known Equation (1) [20].

The calculation of *CLTE* was performed using Equation 2 for each temperature point presented in Table 1. The X-ray diffraction pattern (Fig. 3) shows the reflections (111) of the *CrN* and *ZrN* phases of the multilayer coating in the selected temperature range.

The dependence of the lattice parameter on the temperature is shown in Fig. 4, *a*. The graph shows that the lattice parameter of the coating materials (*CrN* and *ZrN*) increases, indicating an increase in material volume, which occurs according to a linear law with some error. The dependence of the lattice parameter on the exposure temperature is shown in Fig. 4, *b*.

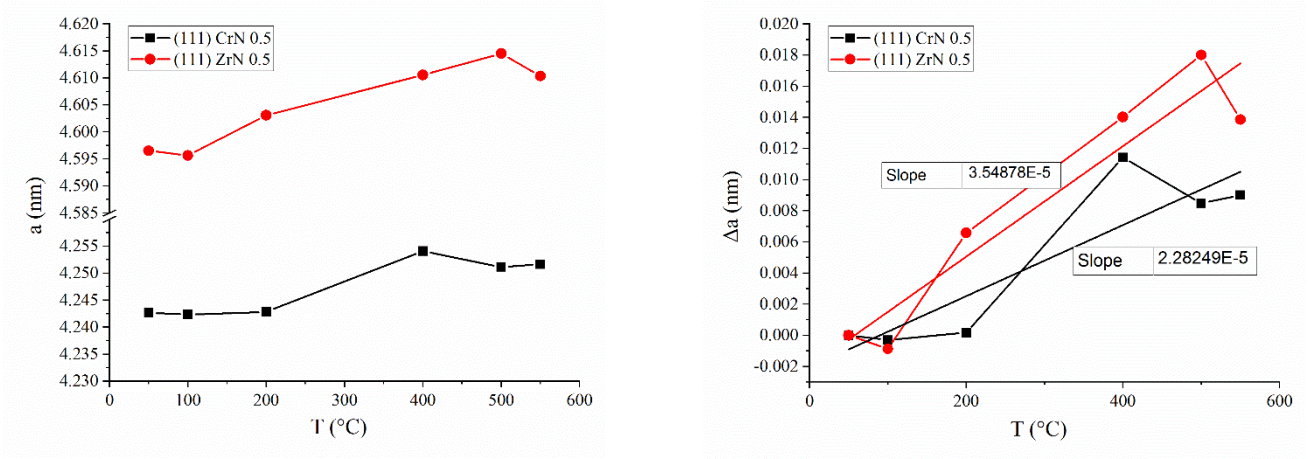

a *b*

Fig. 4. Dependence of the crystal lattice parameter of the *ZrN*/*CrN* multilayer coating phases on temperature – *a*; dependence of the changes in the crystal lattice parameter (Δ*a*) of the phases of the *ZrN*/*CrN* multilayer coating on temperature – *b*

Equation 2 is applied as follows. Obviously, Figure 4b is a modified graph shown in Figure 4a, such that $\Delta a = a_T - a_0$, where a_T is the lattice parameter at a higher temperature (in the case of Figures 4a, b, the highest values on the linear segments: 50–550 °C), and $\boldsymbol{a}_0$ is the lattice parameter at the beginning of the linear segments (in the case of Figures 4a, b, the lowest values on the linear segments: 50–550 °C). That is, for the heating range from 50 °C to 550 °C, the *CLTE* (β) of the *ZrN* phase of the multilayer coating will be calculated as:

$$\beta_{ZrN} = \frac{4,6145 - 4,5965}{4,5965(550 - 50)} = 7,83 \cdot 10^{-6}\ \mathrm{K}^{-1}.$$

For the linear heating range from 50 °C to 550 °C, the lattice constant (β) of the *CrN* phase of the multilayer coating will be calculated as:

$$\beta_{CrN} = \frac{4,2516 - 4,2426}{4,2426(550 - 50)} = 4,24 \cdot 10^{-6}\ \mathrm{K}^{-1}.$$

Equation 2 can be represented graphically as a dependence of the change in the lattice parameter (Δ*a*) on the temperature of exposure, as shown in Fig. 4, *b*. The slope of the tangent in this case is the rate of change of the lattice parameter value (nm) per 1 °C during heating.

The thermal expansion coefficient (*TEC*) over the entire temperature range of exposure from 50 °C to 650 °C will be positive for both phases of the multilayer coating: 2.28249×10^{-14} K^{-1} for the *CrN* phase and 3.54878×10^{-14} K^{-1} for the *ZrN* phase.

Fig. 5 shows the dependence of the *FWHM* of the (111) reflections of the *CrN* and *ZrN* phases on the temperature of exposure. Based on the possibility of the occurrence of microstrains with an increase in the *FWHM* value, it can be concluded that the increase in microstrains is possible in the temperature range

from 50 °C to 400 °C for the *CrN* phase. After reaching the temperature of 400 °C, the *FWHM* value increases and, accordingly, microstrains will also have an increasing dependence for the *CrN* phase. For the *ZrN* phase, the situation is reversed: the *FWHM* value decreases almost throughout the heating process, and accordingly, microstrains will only decrease.

Table 2 presents the calculated values of interplanar distances (*d*, Å), the full width at half maximum (*FWHM*) values (degrees), as well as the calculated lattice parameter for the *CrN*/*ZrN* multilayer coating obtained at a substrate holder rotation speed of 8 rpm using the known Equation 1 [20].

The *CLTE* calculations were performed using Equation 2 for each temperature point presented in Table 1. The X-ray diffraction pattern shows the reflections (111) of the *CrN* and *ZrN* phases of the multilayer coating in the selected temperature range.

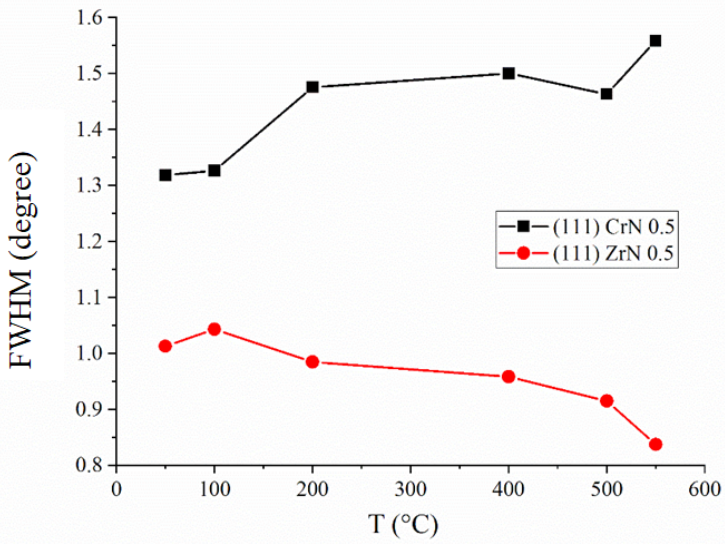

Fig. 5. Dependence of *FWHM* reflection of (111) *CrN* and (111) *ZrN* multilayer coating on temperature

Table 2

Characteristics of reflections of all phases, presented in a sample with a multilayer *CrN*/*ZrN* coating, obtained at a substrate holder rotation speed of 8 rpm as a function of temperature

Temperature, °C	Reflection, phase	*d*, Å	*FWHM*, deg.	*a*, nm
50	(111) *ZrN*	2.6596	1.1329	4.6065
	(111) *CrN*	2.4595	1.5925	4.2599
100	(111) *ZrN*	2.6644	1.0414	4.6148
	(111) *CrN*	2.4679	1.5137	4.2745
200	(111) *ZrN*	2.6671	1.0504	4.6195
	(111) *CrN*	2.4633	1.6553	4.2665
400	(111) *ZrN*	2.6721	1.0941	4.6282
	(111) *CrN*	2.4519	1.6526	4.2468
500	(111) *ZrN*	2.6732	1.0407	4.6301
	(111) *CrN*	2.4595	1.6878	4.2599
550	(111) *ZrN*	2.6729	0.9904	4.6295
	(111) *CrN*	2.4572	1.6518	4.25599524
600	(111) *ZrN*	2.6698	0.8949	4.62422925
	(111) *CrN*	2.4739	1.652	4.28492049

The dependence of the crystal lattice parameter on the temperature is shown in Fig. 6, *a*. From the graph, it can be seen that the crystal lattice parameter of the coating materials (*CrN* and *ZrN*) increases, i.e., the material expands, and this occurs according to a linear law with some error. The dependence of the crystal lattice parameter change on the temperature of the coating materials (*CrN* and *ZrN*) is shown in Fig. 6, *b*.

Equation 2 is applied as follows. Obviously, Fig. 6, *b* is a rearranged graph shown in Fig. 6, *a*, such that $\Delta a = a_T - a_0$, where a_T is the lattice parameter at a higher temperature (in the case of Figures 6, *a*, *b*, the highest values on the linear segments: 50–550 °C), and a_0 is the lattice parameter at the beginning of the linear segments (in the case of Figures 6, *a*, *b*, the lowest values on the linear segments: 50–550 °C). Thus,

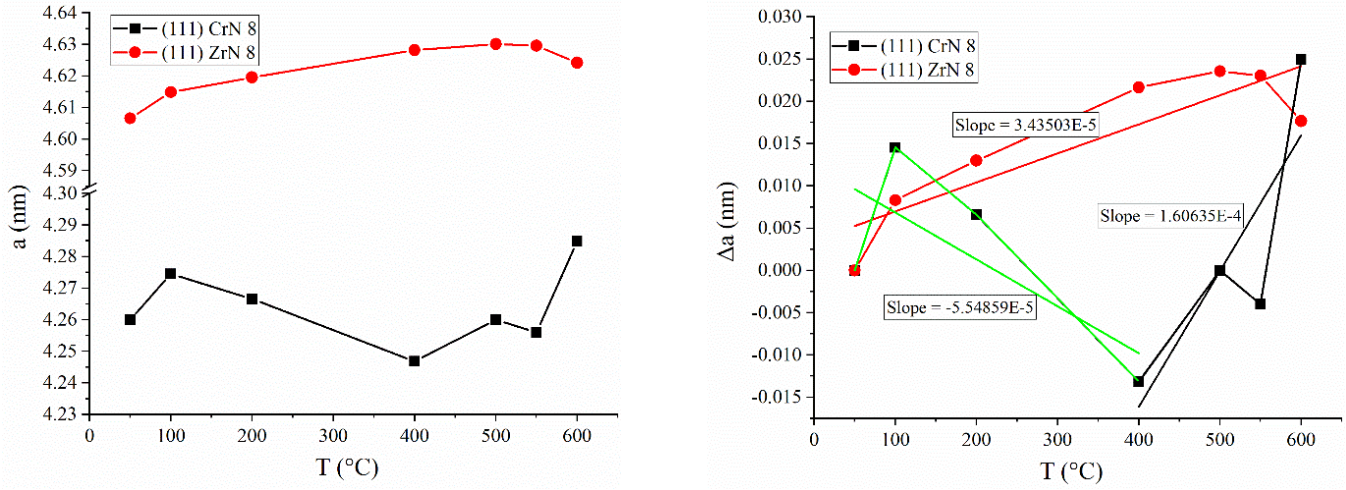

a *b*

Fig. 6. Dependence of the changes in the crystal lattice parameter of the phases of the *ZrN*/*CrN* multilayer coating on temperature – *a*; dependence of the changes in the crystal lattice parameter (Δ*a*) of the phases of the *ZrN*/*CrN* multilayer coating on temperature – *b*

for the heating range from 50°C to 550°C, the *XRD* (β) of the *ZrN* phase of the multilayer coating will be calculated as:

$$\beta_{ZrN} = \frac{4,6242 - 4,6065}{4,6065(600 - 50)} = 6,99 \cdot 10^{-6}\,\mathrm{K}^{-1}.$$

In the case of the *CrN* coating component, it can be seen from Fig. 3a that the dependence is not linear but consists of two linear segments.

The first segment is 50–400 °C, and for it, the *CLTE* should be calculated separately. For the linear heating range from 50 °C to 550 °C, the lattice constant (*β*) of the *CrN* phase of the multilayer coating will be calculated as:

$$\beta_{CrN} = \frac{4,2468 - 4,2599}{4,2599(400 - 50)} = -8,79 \cdot 10^{-6}\,\mathrm{K}^{-1}.$$

In the temperature range from 50 °C to 400 °C, the component of the C*r*N multilayer coating undergoes compression.

The second section, from 400 °C to 600 °C, should also be calculated separately. For this linear heating range, the lattice constant of the *CrN* phase of the multilayer coating (β) is calculated as:

$$\beta_{CrN} = \frac{4,2849 - 4,2468}{4,2468(600 - 400)} = 4,49 \cdot 10^{-5}\,\mathrm{K}^{-1}.$$

In the temperature range of heating from 400°C to 600°C, the expansion of the component of the *CrN* multilayer coating occurs, but the *CLTE* of the *CrN* component is an order of magnitude higher than that of the *ZrN* component of the multilayer coating.

For clarity, Equation 2 can be represented in graphical form as a dependence of the change in the lattice parameter (*Δa*) on the temperature of exposure, as shown in Fig. 6b. The tangent of the slope angle in this case is the rate of change in the value of the lattice parameter (nm) per 1 °C during heating.

The *CLTE* value for *ZrN* phase in the temperature range of 50 °C to 600 °C is positive and equals 3.44×10^{-5} nm/K, as shown above the red straight line. For the *CrN* phase of the multilayer coating, in the temperature range of 50 °C to 400 °C, the *CLTE* value corresponds to a negative value of -5.55×10^{-5} nm/K. The positive *CLTE* value is observed in the temperature range of 400 °C to 600 °C, and it equals 1.61×10^{-4} nm/K for the *CrN* phase of the multilayer coating.

Figure 7 shows the plot of the dependence of *FWHM* of (111) *CrN* and (111) *ZrN* phase reflections on the temperature. Based on the possibility of the occurrence of microstresses with an increase in the *FWHM* value, it can be concluded that microstresses can occur to a small extent for the *CrN* phase of the multilayer coating up to 200 °C. After reaching the temperature of 200 °C, the *FWHM* value remains, on average, at the same level. For the *ZrN* coating component, the *FWHM* value slightly increases up to the temperature of 400 °C, and then the *FWHM* value decreases, accordingly, microstresses will also have a decreasing dependence.

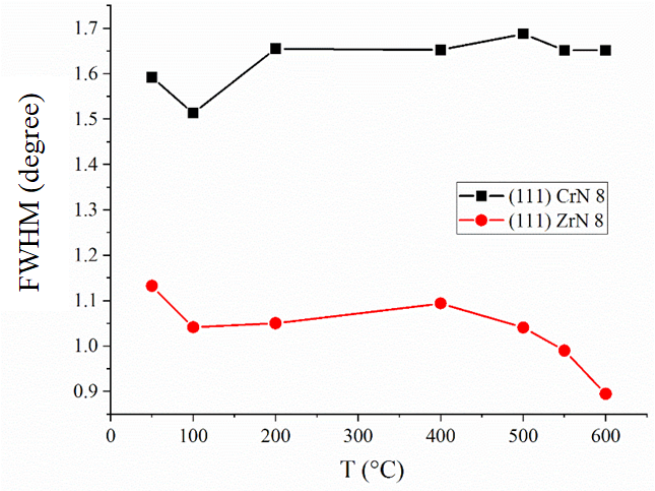

Fig. 7. Dependence of *FWHM* reflection of (111) *CrN* and (111) *ZrN* multilayer coating on temperature

As a result of the sequential actions with obtaining X-ray diffraction patterns of samples with coatings under temperature exposure, sampling and evaluation of X-ray diffraction patterns according to the proposed algorithm, recommendations for the application of coating technologies depending on the parameters of coating application can be made.

The recommendations consist of a two-stage algorithm, consisting of:

1. Determining the *CLTE* of individual coating components;
2. Determining the *FWHM* and comparing it with the *FWHM* minimum of two samples with coatings.

If the calculated *CLTE* values for some coating components exhibit differences, the deposition mode in which the *CLTE* of coating components exhibits the minimum differences at any temperature is selected as the optimal deposition mode. The temperature, at which the *CLTE* of coating components exhibits the minimum differences or is equal, is selected as the optimal mode of multilayer deposition, and the coating in which the *FWHM* values, as determined by the X-ray profile approximation, exhibit a decreasing dependency, is most suitable for prolonged use due to the minimal microstresses existing in the coating.

Conclusions

Based on the conducted research using the proposed algorithm, conclusions and recommendations can be made regarding the application and use of *CrN*/*ZrN* coatings:

A multilayer coating of *CrN*/*ZrN* deposited at a table rotation speed of 0.5 revolutions per minute (*rpm*) had varying *CLTE* values throughout the entire thermal testing, with differences in *CLTE* between components exceeding 50%. For the multilayer coating deposited at a table rotation speed of 8 rpm, the *CLTE* dependence was found to be linear only for the *CrN* component, while the *ZrN* component exhibited an extremum in the temperature range of 400 °C. Prior to heating the coating to 400 °C, the *CLTE* was negative, and after reaching 400 °C, it changed sign to positive. This indicates that within a narrow temperature range around 400 °C, the *CLTE* of both coating components will not differ significantly. Therefore, the coating application mode with a table rotation speed of 8 rpm will be optimal.

Based on the *FWHM* data, the occurrence of microstresses is possible for both coating application modes (0.5 and 8 rpm). However, for the coating application mode with a table rotation speed of 8 rpm, no microstresses were observed for the *CrN* component, even after exposure to 500 °C. This leads to the conclusion that this deposition mode for the multilayer coating is optimal.

References

1. Liu J., Hao Z., Cui Z., Ma D., Lu J., Cui Y., Li C., Liu W., Xie S., Hu P., Huang P., Bai G., Yun D. Oxidation behavior, thermal stability, and the coating/substrate interface evolution of CrN-coated Zircaloy under high-temperature steam. *Corrosion Science*, 2021, vol. 185, p. 109416. DOI: 10.1016/j.corsci.2021.109416.

2. Pashkov D.M., Belyak O.A., Guda A.A., Kolesnikov V.I. Reverse engineering of mechanical and tribological properties of coatings: results of machine learning algorithms. *Physical Mesomechanics*, 2022, vol. 25, pp. 296–305. DOI: 10.1134/S1029959922040038.

3. Manaud J.P., Poulon A., Gomez S., Petitcorps Y.L. A comparative study of CrN, ZrN, NbN and TaN layers as cobalt diffusion barriers for CVD diamond deposition on WC–Co tools. *Surface and Coatings Technology*, 2007, vol. 202, pp. 222–231. DOI: 10.1016/j.surfcoat.2007.05.024.

4. Lee D.B., Lee Y.C., Kwon S.C. High temperature oxidation of TiCrN coatings deposited on a steel substrate by ion plating. *Surface and Coatings Technology*, 2001, vol. 141, pp. 232–239. DOI: 10.1016/S0257-8972(01)01237-3.

5. Kolubaev A.V., Sizova O.V., Denisova Y.A., Leonov A.A., Teryukalova N.V., Novitskaya O.S., Byeli A.V. Structure and properties of CrN/TiN multilayer coatings produced by cathodic arc plasma deposition on copper and beryllium-copper alloy. *Physical Mesomechanics*, 2022, vol. 25, pp. 306–317. DOI: 10.1134/S102995992204004X.

6. Liu J., Tang C., Steinbrück M., Yang J., Stegmaier U., Große M., Yun D., Seifert H.J. Transient experiments on oxidation and degradation of Cr-coated Zircaloy in steam up to 1600 C. *Corrosion Science*, 2021, vol. 192, p. 109805. DOI: 10.1016/j.corsci.2021.109805.

7. Kashkarov E.B., Sidelev D.V., Syrtanov M.S., Tang C., Steinbrück M. Oxidation kinetics of Cr-coated zirconium alloy: Effect of coating thickness and microstructure. *Corrosion Science*, 2020, vol. 175, p. 108883. DOI: 10.1016/j.corsci.2020.108883.

8. Hu D., Fu Q., Li X., Zhou L., Zhang J. Discussion on structural parameters of the multilayer ZrC/TaC coatings based on stress analysis and ablation behaviors. *Surface and Coatings Technology*, 2022, vol. 435, p. 128243. DOI: 10.1016/j.surfcoat.2022.128243.

9. Chen Y.I., Lo H.H., Ke Y.E. Thermal stability of laminated Ru–Al/Ru–Si–Zr coatings on Inconel 617. *Surface and Coatings Technology*, 2020, vol. 399, p. 126194. DOI: 10.1016/j.surfcoat.2020.126194.

10. Sidelev D.V., Syrtanov M.S., Ruchkin S.E., Pirozhkov A.V., Kashkarov E.B. Protection of Zr alloy under high-temperature air oxidation: a multilayer coating approach. *Coatings*, 2021, vol. 11, p. 227. DOI: 10.3390/coatings11020227.

11. Boretius M., Krappitz H., Rass I. Wear protection coatings generated by brazing, sintering and heat treatment in vacuum. *Tribologie und Schmierungstechnik*, 2017, vol. 64, pp. 35–9.

12. Gérard B. Application of thermal spraying in the automobile industry. *Surface and Coatings Technology*, 2006, vol. 201, pp. 2028–2031. DOI: 10.1016/j.surfcoat.2006.04.050.

13. Bobzin K., Brögelmann T., Kalscheuer C., Liang T. High-rate deposition of thick (Cr,Al)ON coatings by high speed physical vapor deposition. *Surface and Coatings Technology*, 2017, vol. 322, pp. 152–162. DOI: 10.1016/J.SURFCOAT.2017.05.034.

14. Kolesnikov V.I., Kudryakov O.V., Zabiyaka I.Y., Novikov E.S., Manturov D.S. Structural aspects of wear resistance of coatings deposited by physical vapor deposition. *Physical Mesomechanics*, 2020, vol. 23, pp. 570–583. DOI: 10.1134/S1029959920060132.

15. Xia F., Xu H., Liu C., Wang J., Ding J., Ma C. Microstructures of Ni–AlN composite coatings prepared by pulse electrodeposition technology. *Applied Surface Science*, 2013, vol. 271, pp. 7–11. DOI: 10.1016/j.apsusc.2012.12.064.

16. Krysina O.V., Ivanov Y.F., Koval N.N., Prokopenko N.A., Shugurov V.V., Petrikova E.A., Tolkachev O.S. Composition, structure and properties of Mo-N coatings formed by the method of vacuum-arc plasma-assisted deposition. *Surface and Coatings Technology*, 2021, vol. 416, p. 127153. DOI: 10.1016/j.surfcoat.2021.127153.

17. Li Z., Liu C., Chen Q., Yang J., Liu J., Yang H., Zhang W., Zhang R., He L., Long J., Chang H. Microstructure, high-temperature corrosion and steam oxidation properties of Cr/CrN multilayer coatings prepared by magnetron sputtering. *Corrosion Science*, 2021, vol. 191, p. 109755. DOI: 10.1016/j.corsci.2021.109755.

18. Khamseh S., Araghi H. A study of the oxidation behavior of CrN and CrZrN ceramic thin films prepared in a magnetron sputtering system. *Ceramics International*, 2016, vol. 42, p. 9988–9994. DOI: 10.1016/j.ceramint.2016.03.101.

19. PseudoVoigt, (n.d.). Available at: https://docs.mantidproject.org/nightly/fitting/fitfunctions/PseudoVoigt.html (accessed 11.04.2023).

20. Gorelik S.S., Rastorguev L.N., Skakov Yu.A. *Rentgenograficheskii i elektronnoopticheskii analiz* [X-Ray diffraction and electron-optical analysis]. 2nd ed. Moscow, Metallurgiya Publ., 1970. 366 p.

21. Rusakov A. *Rentgenografiya metallov* [Metal radiography]. Moscow, Atomizdat Publ., 1977. 480 p.

Conflicts of Interest

The authors declare no conflict of interest.